JGR Oceans

RESEARCH ARTICLE
10.1029/2019JC015856

The Summer Heat Balance of the Oregon Inner Shelf Over Two Decades: Mean and Interannual Variability

E. Lemagie[1], **A. Kirincich**[1], **and S. Lentz**[1]

[1]Woods Hole Oceanographic Institution, Woods Hole, MA, USA

Key Points:
- Inner-shelf temperatures are approximately constant despite strong surface heating during summer
- The across-shelf heat exchange balances the surface heat flux over the inner shelf most years
- There is significant interannual variability in the across-shelf heat exchange during summer

Correspondence to:
E. Lemagie,
elemagie@whoi.edu

Citation:
Lemagie, E., Kirincich, A., & Lentz, S. (2020). The summer heat balance of the Oregon inner shelf over two decades: Mean and interannual variability. *Journal of Geophysical Research: Oceans*, *125*, e2019JC015856. https://doi.org/10.1029/2019JC015856

Received 6 NOV 2019
Accepted 15 JAN 2020
Accepted article online 24 JAN 2020

Abstract Summer temperature and velocity measurements from 14 years in 15 m of water over the inner shelf off Oregon were used to investigate interannual temperature variability and the capacity of the across-shelf heat flux to buffer net surface warming. There was no observable trend in summer mean temperatures, and the standard deviation of interannual variability (0.5°C) was less than the standard deviation in daily temperatures each summer (1.6°C, on average). Yet net surface heat flux provided a nearly constant source of heat each year, with a standard deviation less than 15% of the interannual mean. The summer mean across-shelf upwelling circulation advected warmer water offshore near the surface, cooling the inner shelf and buffering the surface warming. In most years (11 out of 14), this two-dimensional heat budget roughly closed with a residual less than 20% of the leading term. Even in years when the heat budget did not balance, the observed temperature change was negligible, indicating that an additional source of cooling was needed to close the budget. A comparison of the residual to the interannual variability in fields such as along-shelf wind stress, stratification, and along-shelf currents found no significant correlation, and further investigation into the intraseasonal dynamics is recommended to explain the results. An improved understanding of the processes that contribute to warming or cooling of the coastal ocean has the potential to improve predictions of the impact of year-to-year changes in local winds and circulation, such as from marine heat waves or climate change, on coastal temperatures.

Plain Language Summary Long-term observations over 14 summer seasons at a site off the Oregon coast were used to understand the year-to-year changes in the ocean temperatures between 1 km offshore in 15 m of water and the shoreline. The summer mean temperature did not change at this site, and year-to-year changes in the summer mean temperature were less than the variability in the temperature within a single year. Warming at the surface, such as from solar heating, was also relatively consistent from year to year. A simple budget was presented to estimate the relative contributions of different processes that can warm or cool the water. The summer mean circulation pattern in the across-shelf direction, which transports warmer water offshore near the surface, cooled the inner shelf and buffered or balanced the surface warming in most years. It was not clear what other processes contribute to warming or cooling of the coastal ocean, but additional work is needed to understand the potential impact of year-to-year changes in the local winds and circulation, such as from marine heat waves or climate change, on coastal temperatures.

1. Introduction

The heating and cooling of the inner part of the continental shelf by processes such as air-sea exchange or advection play a dominant role in setting the temperature of this critical region of the coastal ocean. Changes in coastal ocean temperatures can have important biological implications. Small shifts in nearshore oceanic temperatures have been shown to lead to substantial changes in species composition and predator/prey interactions (Keller et al., 1999; Sanford, 1999), physiological adaptations (Somero, 2005), and disease persistence (Cook et al., 1998). Many species, particularly in temperate marine ecosystems, live at the upper edge of their thermal tolerance (Somero, 2005) and are highly susceptible to mass mortality events due to increased coastal temperatures and/or alterations in the dominant circulation processes (Barth et al., 2007; Sydeman et al., 2006). Thus, our ability to predict changes in nearshore water temperatures under a range

of climate change scenarios depends on having detailed knowledge of how the sources and sinks of heat contribute to an overall budget of temperature in the coastal ocean.

On the U.S. West Coast, shelf-wide temperatures exhibit a seasonal cycle, with the lowest surface temperatures in summer (Huyer, 1977). Following a rapid $\mathcal{O}$(1 week) spring transition, resulting from the cumulative offshore Ekman transport due to upwelling-favorable winds, lateral density gradients and vertically sheared horizontal currents tend to persist for the rest of the summer, even during moderate downwelling-favorable wind events (Huyer et al., 1979). The onset of upwelling-favorable winds is highly variable from year to year (Bylhouwer et al., 2013), but shifts in the timing or the strength of the upwelling impacts the temperature of the shelf as well as nutrient levels and productivity observed over the shelf in summer (Barth et al., 2007). At interannual time scales, weaker upwelling winds and/or shorter upwelling seasons correlate with positive phases of the Pacific Decadal Oscillation (PDO). Warm phases of the El Niño Southern Oscillation (ENSO) index have also been associated with a later onset of summer upwelling as well as more intense downwelling (Bylhouwer et al., 2013; Frischknecht et al., 2015). The combination of these two patterns of climactic variability may also lead to the observation of more extreme events along the coast (Smith et al., 2001), such as the marine heatwave that occurred between 2014 and 2016 (Di Lorenzo & Mantua, 2016; Gentemann et al., 2016).

Previous studies have indicated that the heat budget in these regions is dominated by a two-dimensional balance where the offshore advective heat flux due to wind-driven upwelling buffers warming due to the net surface heat flux over the midshelf in summer (Bryden et al., 1980; Dever & Lentz, 1994; Lentz, 1987; Send, 1989). Along-shelf variations in the strength of the coastal upwelling are reflected by the along-shelf temperature distribution (Huyer, 1983). For comparison, while the summer heat budget in these regions is dominated by a two-dimensional balance, this becomes more three-dimensional in the wintertime (Dever & Lentz, 1994) when along-shelf heat fluxes are increasingly important (Rudnick & Davis, 1988).

However, closer to shore, the midshelf to inner-shelf summer temperatures exhibit little or no interannual variability and have only weak relationships with the local winds (Hickey et al., 2016). Here, wind-driven Ekman transport is reduced relative to midshelf as is the along-shelf flow due to the presence of the coast (Gill, 1982; Kirincich et al., 2005; Lentz, 2001), potential decreases in along-shelf wind stress and pressure gradients, as well as increased bottom drag in shallower water (Lentz, 1994). A similar two-dimensional summer heat balance has been observed over the inner shelf on the U.S. East Coast by Fewings and Lentz (2011) who found persistent cooling due to a mean upwelling circulation which was not wind-driven. However, the role of offshore advection in buffering the surface heat flux on wind-driven inner shelves is not fully understood. For example, despite significantly warmer ocean temperatures in the surrounding region, sea surface temperatures (SSTs) near the Oregon coast were not abnormal during the 2014–2016 heat wave described above.

Although coastlines with predominantly upwelling-favorable winds in summer are known for their low water temperatures (Summerhayes et al., 1995), the role of the across-shelf heat flux on the inner-shelf heat budget has not been quantified at seasonal or interannual timescales. While it is likely that across-shelf circulation is important to the inner-shelf heat balance, few studies of the inner-shelf heat balance along the West Coast exist, except at diurnal time scales (Suanda et al., 2011), partially because long-term, co-located records of inner-shelf temperatures and velocities rarely exist. In addition, the difficulty of acquiring accurate surface heat flux measurements often hinders the ability to close oceanic heat budgets (Lentz et al., 2003).

This study investigates the variability of inner-shelf ocean temperatures on seasonal and interannual timescales and the roll of advection in buffering the surface heat flux. Summer observations from an inner-shelf site spanning nearly 20 years and a high-resolution global reanalysis of surface heat flux are used in order to quantify the interannual temperature variability along a relatively straight wind-driven coastline. These observations are also used to construct a two-dimensional heat budget in order to quantify the contribution of the across-shelf heat flux to cooling the inner shelf. This unique set of long-term observations of water column temperature and velocity measurements come from the Partnership for the Interdisciplinary Studies of Coastal Ocean's (PISCO) Oregon State University (OSU) mooring program. The PISCO program is a long-term ecological consortium created in 1998 to study the link between inner-shelf oceanography and marine ecosystems along the U.S. West Coast. The objectives of the program are to quantify patterns of distribution, abundance, and diversity in nearshore communities and determine how oceanographic processes influence these patterns.

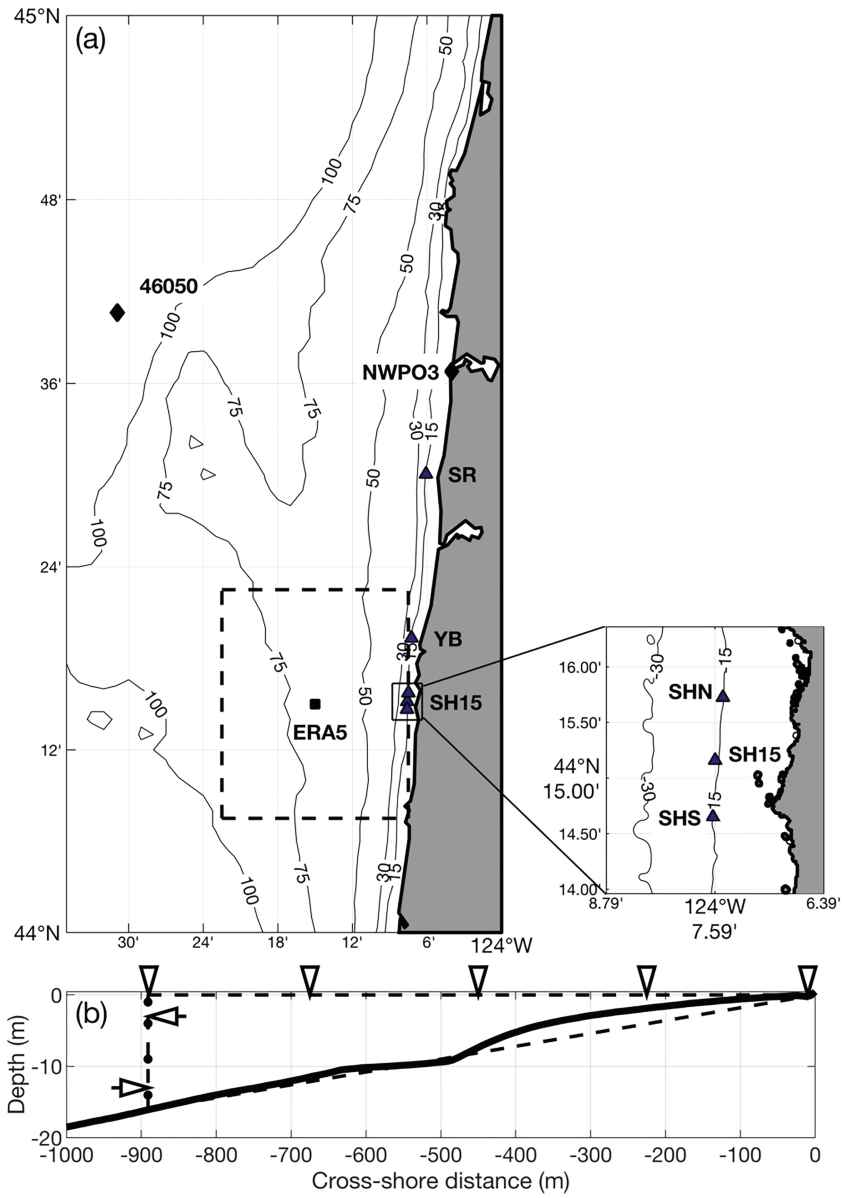

Figure 1. (a) A map of the central Oregon coasts showing the PISCO sites around Strawberry Hill (SHS, SH15, and SHN), Yachats Beach (YB), and Seal Rock (SR) along with the location of NDBC data buoys and the nearest ERA5 grid point. (b) A cross section of the measured bathymetry cross section between the SH15 and the coast relative to a linear sloping bathymetry assumed in a simple two-dimensional model. Arrows represent the spatially uniform heat flux across the surface and the depth-varying heat flux at the offshore boundary. Dots at the offshore boundary represent the depths of the temperature sensors.

The Oregon coast is particularly well situated for an examination of the inner-shelf heat budget. The shelf-wide dynamics are upwelling-favorable, and thus, across-shelf exchange is likely to be large. The PISCO observational site in 15-m of water is located adjacent to a relatively straight alongshore stretch of the coastline. Nearby coastal surface heat flux estimates that span the full period are available from the recently published European Centre for Medium-Range Weather Forecasts (ECMWF) fifth global reanalysis (herein referred to as ERA5). The study is organized as follows. In section 2 we describe the data and the heat budget calculation. The interannual variability in the heat budget is described in section 3, as well as the interannual variability in the forcing fields that are likely to impact the advection and accumulation of heat over the inner shelf. In section 4 we discuss the uncertainty in the heat budget estimates and additional terms, such as along-shelf advection, that might be necessary to close the budget when across-shelf heat advection does not balance the surface heat flux.

2. Data and Methods

2.1. PISCO Observing Program

The primary focus of this paper is on data collected from inner-shelf location SH15 over 18 summers (Figure 1a). SH15 is less than 1 km offshore (−124.13°, 44.25°), adjacent to a region where the coastline is predominantly aligned in the north-south direction. The summer data collection season ranges from April to September.

Velocity and temperature data were collected over the summer months at multiple 15-m depth stations as part of the long-term PISCO observational effort. The PISCO mooring array (Figure 1a) includes stations near Seal Rock (SR), Yachats Beach (YB), and group of moorings offshore of Strawberry Hill (SH15, SHN to the north, and SHS to the south). SH15 has been occupied the longest of all PISCO inner-shelf stations, with summer velocity and temperature time series collected each year from 2000 to 2017. However, years 2001 and 2010 were excluded from this analysis because of data availability or quality control issues. Temperatures were recorded at SHN and SHS beginning in 2003 through 2017 and 2011, respectively, and at sites SR and YB from 2002 to 2009 and 2000 to 2009, respectively.

At each site, temperature was measured at four depths including at 1 m below a surface-mounted float and from sensors at 1, 6, and 11 m above a bottom-mounted mooring (Figure 1b). From 1998 to 2007, StowAway XTI and Tidbit V2 temperature sensors from Onset Computer Corp. were used, which were replaced with Onset HOBO U22 Water Temp Pro V2 sensors between 2008 and 2009. Each of these sensors has an accuracy of around 0.2°C (Lentz et al., 2012). All temperature sensors were sampled at 2 min.

A bottom-mounted upward looking RDI Workhorse Sentinel 600-kHz acoustic Doppler current profiler (ADCP) was deployed alongside the temperature mooring at sites SR, YB, and SH15. However, only velocities at SH15 are used for this study. Velocities were averaged over 1 m bins in depth and at 2 min time intervals, although this study utilizes an hourly averaged product for both temperature and velocity.

2.2. Data Processing

2.2.1. Sea Surface Height

Time series of hourly sea surface height (SSH) were derived from the pressure and acoustic intensity observations collected by the ADCPs. To estimate SSH, the backscatter intensity from all four beams was summed, and the water surface was identified as the depth of the maximum beam intensity from a parabolic fit. Quality control was also performed by removing points from the high frequency residual (after running a Loess smoothing filter with a span of $\frac{1}{2}$-day) that were more than 3 standard deviations from the mean for each deployment. From 2004 onwards, the pressure and intensity fields were used to estimate SSH; prior to 2004, when pressure was not available, only intensity was used. The estimated accuracy of SSH was ∼10 cm. A pressure-based estimate of SSH was used whenever direct observations of sea-level pressure were available, due to its smaller associated error. The accuracy for the ADCPs pressure sensor was ∼1.5–3.8 cm (depending on water depth). The largest source of error in the pressure measurement was the predeployment offset. In order to account for this offset, the pressure-derived SSH was calibrated by subtracting the difference between the deployment-averaged intensity-derived SSH and pressure time series. These estimates of SSH were used to transform the current and temperature profiles into a σ-coordinate grid with 18 evenly spaced σ levels so that each level has a bin depth of roughly $\leq$1 m. Hourly temperature and velocity fields were interpolated onto this grid in order to aid in the calculation of the depth-averaged and flux estimates.

2.2.2. Temperature Measurements

Initial quality control was performed by removing large anomalies (greater than 3 standard deviations beyond the record-mean value) from each temperature record. Individual data gaps of 6 hr or less were linearly interpolated. This interval was chosen by inspection as the minimum time-lagged autocorrelation was high (greater than 0.6) at less than 6 hr. Each time series was also compared to the ADCP temperature sensor (if available) and surface temperatures from NDBC buoy 46050 (Figure 1) to confirm that no cross-correlation lag existed, which would indicate an error in synchronizing the instrument clocks. For the temperature observations at SH15, temperature data from all four sensors as well as ADCP velocities spanning the water column were required for each time in the analyzed data record (e.g., the time series of daily-averaged, depth-averaged temperatures, $\hat{T}$, are shown in Figure 2). At all other sites, only the surface and bottom temperatures were required to be available, but each summer of data was required to have greater than a 50% overlap with the SH15 processed record.

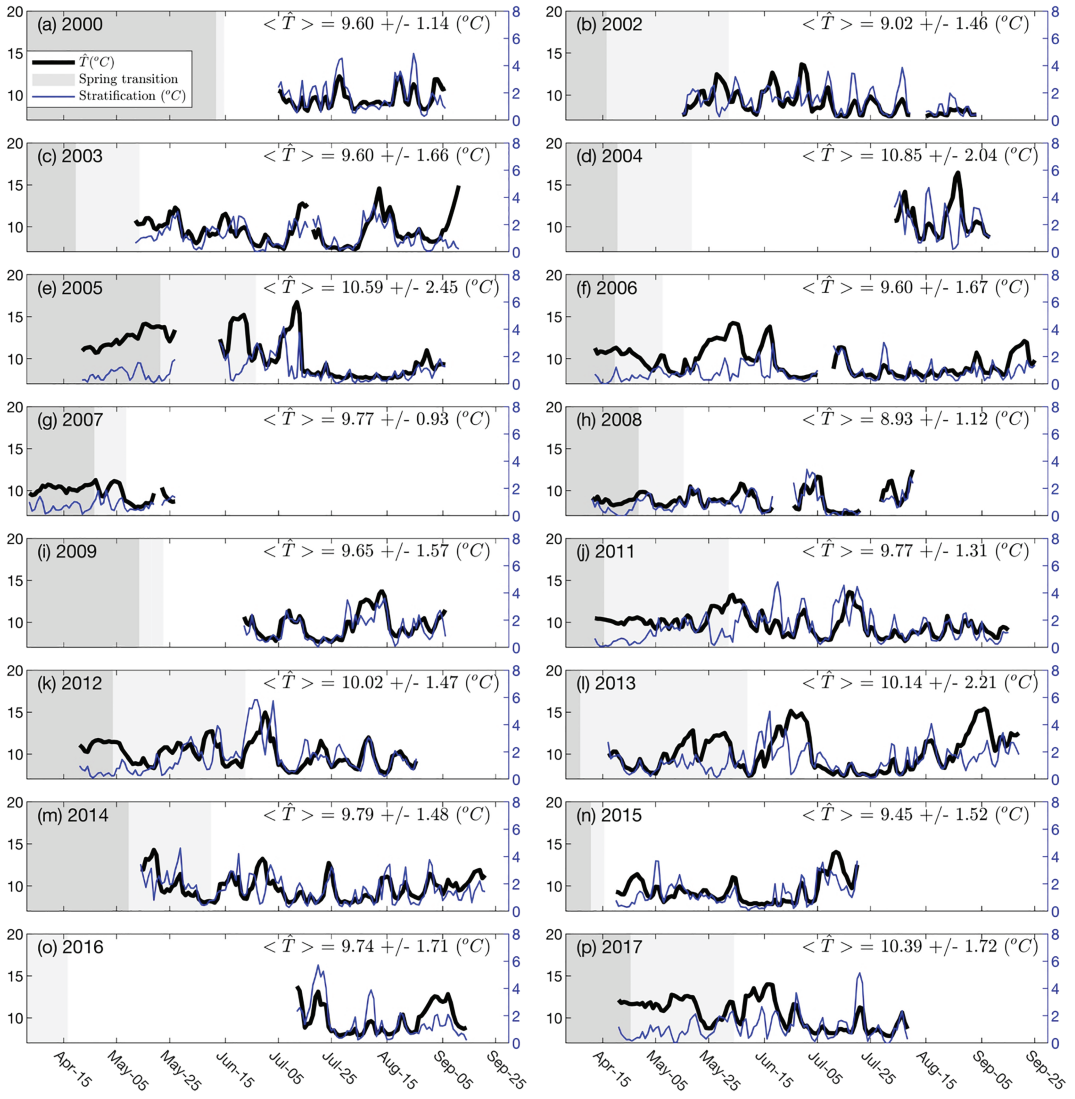

Figure 2. Daily-averaged, depth-averaged temperature, $\hat{T}$, and the top-to-bottom temperature difference at SH15 (thin blue lines) for each summer season. Gray shading indicates the timing, and 95% confidence interval, of the spring transition, based on an index by Pierce and Barth (http://damp.coas.oregonstate.edu/windstress/index.html).

As a result of these quality control requirements, years 2001 and 2010 were excluded due to a lack of ADCP velocity measurements. In 2004, the surface mooring sank in the early-season deployment, resulting in no coverage of the top of the water column. Additionally, the record lengths from the summers of 2004 and 2007 were both less than 60 days—notably shorter than other years—and these years were also excluded. Except in 2005, nearly the entirety of the record each season was after the estimated timing of the spring transition to upwelling-favorable wind conditions (Figure 2). Summer means were then defined as the mean of all available data each year, which only includes times when temperature, velocity, and surface heat flux data were all present.

At SH15, temperature data were linearly interpolated onto the depth-following σ-coordinate grid. Values within 1 m of the surface and bottom were extrapolated using a "well-mixed" approximation at each hourly measurement. This approximation does not appreciably change the summer mean temperature profile since the measurements span most of the water column (e.g., Figure 3a).

2.2.3. Velocity Profiles

ADCP velocities within 10% of the water depth of the surface and above were masked due to side lobe reflection (Gordon, 1996), as were values within 2 m of the instrument. Processed velocity data were linearly interpolated onto the "tide-following" σ-coordinate grid. In order to compute across-shelf fluxes over the

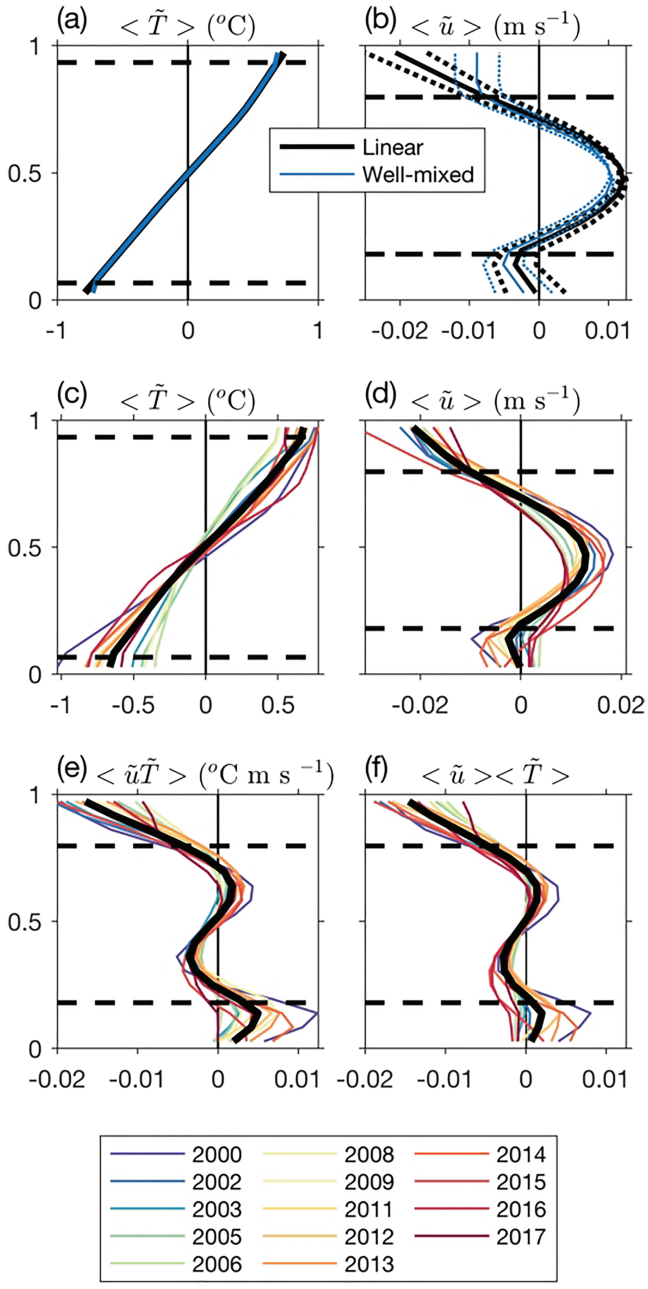

Figure 3. Example summer mean profiles of (a) temperature and (b) velocity variability with depth under different extrapolation assumptions and the sensitivity to axis rotation, taken from 2009. The summer mean profiles of (c) $\tilde{T}$, (d) $\tilde{u}$, (e) $< \tilde{u}\tilde{T} >$, and (f) $< \tilde{u} >< \tilde{T} >$ are also shown, with colors showing the interannual variability between years and the interannual mean in black. Horizontal dashed lines indicate the vertical observation limits.

entire water column, velocities were extrapolated to the surface and bottom (e.g., Figure 3b). Values within 2.7 m of the bottom were estimated by linearly interpolating to 0 m s^{-1} at the bottom. The extrapolation distance to the surface varied over time and ranged between 3 ± 1 m below sea level. Two methods of extrapolating near-surface values were compared: (1) a "well-mixed" extrapolation where near-surface values were the same as the shallowest measurement and (2) a linear extrapolation where near-surface values were derived using a linear fit between the two shallowest measurements. The well-mixed assumption resulted in smaller offshore velocities at the surface (e.g., Figure 3b). However, a comparison of the across-shelf surface Ekman transport integrated to the first zero crossing of the velocity profile to the predicted transport based on the along-shelf wind stress was similar for both methods. Regardless of the extrapolation method,

the profile of $< \tilde{u} >$ was qualitatively similar across all years (Figure 3d). Note that nonzero values at the seafloor are indicative of $< \hat{u} >$, as the linear extrapolation to 0 velocity at the seafloor was calculated before decomposing u into its depth-averaged and depth-varying components.

ADCP velocities were then rotated into the principal axis coordinate system, defined by minimizing the depth-averaged velocity variance in the across-shelf direction. The mean principal axis rotation angle for each individual deployment at SH15 was 4° ± 5° clockwise from north. Velocities near the surface and the bottom were more sensitive to rotation than midwater column velocities (e.g., Figure 3b). If the rotation angle was varied by ±5°, the average change in the seasonally averaged depth-varying across-shelf velocity, $< \tilde{u} >$, at the surface was 0.005 m s^{-1}, $\mathcal{O}(20\%)$ of the water velocity, and 0.003 m s^{-1} at the bottom. Although the across-shelf velocity shear and transport can be sensitive to this rotation angle, this method of estimating the principal axes by minimizing across-shelf variance is standard practice (e.g., Kirincich et al., 2005). These estimates were compared to estimates of the along-shelf orientation of the coastline and the 15-m isobath over a 4-km span centered at SH15. The principal axis rotation angle of 4° ± 5° clockwise from north was similar to the estimated angle of the coastline (8° ± 2°) and the estimated angle of the 15-m isobath (3° ± 0.1°).

2.3. Surface Heat Flux

Surface heat flux was estimated using hourly data at the nearest grid point of the ERA5 reanalysis (European Centre for Medium-Range Weather Forecasts, 2019, Figure 1a). This grid point was roughly 10 km offshore of SH15 in 70-m water depth. Net solar radiation, incoming thermal radiation, surface pressure, 10-m wind speeds, 2-m temperature, and dewpoint temperature from ERA5 along with SST from SH15 were used to calculate the net surface heat flux following Fairall et al. (2003). As described in Appendix A, the ERA5 reanalysis was found to be the most relevant estimate of surface heat flux for this study.

2.4. Other Data Sources

Bathymetry data from the 2008 NOAA 1/3 arc-second Central Oregon Coast Digital Elevation Model (https://catalog.data.gov/dataset/central-oregon-coastal-digital-elevation-model) were used to determine the inner-shelf profile (Figure 1b). Observations of surface winds and water temperatures were obtained from the National Data Buoy Centers (NDBC) midshelf station 46050 and the Coastal Marine Automated Network (CMAN) station NWPO3 (Figure 1). NDBC buoy 46050 is located at 33 km offshore of Newport, Oregon, in 100 m of water. Station NWPO3 is located on the south jetty of the Newport harbor entrance. Hourly wind velocities corresponding with each SH15 deployment were rotated onto the principal axes of the depth-averaged currents to distinguish along-shelf and across-shelf surface stresses. The annual timing of the spring transition to predominantly upwelling-favorable winds was obtained (from http://damp.coas.oregonstate.edu/windstress/index.html), based on the index of Pierce and Barth (Barth et al., 2007; Pierce et al., 2006).

2.5. Heat Budget

As a framework for studying the processes controlling inner-shelf temperature, the heat budget in an across-shelf section was examined (Figure 1b). Integrating from the surface ($z = 0$) to the bottom ($z = -H(x)$) and from the mooring location ($x = -L$) to the coast ($x = 0$), the heat budget may be written as

$$\frac{\partial}{\partial t}\int\int TdA = \int_{-L}^{0}\frac{Q}{\rho_o C_P}dx + \int_{-H}^{0} uTdz\Big|_{x=-L} - \int\int\frac{\partial(vT)}{\partial y}dA, \quad (1)$$

where T is temperature, A is the across-sectional area onshore of the mooring, u, v are the across- and along-shelf velocity, Q is the surface heat flux, ρ_o = 1,024.6 kg m^{-3} is the reference density, and C_P is the heat capacity of seawater. Decomposing u and T into depth-averaged and depth-dependent components ($u = \hat{u} + \tilde{u}, T = \hat{T} + \tilde{T}$) in the across-shelf advective term and T into the cross-sectional area average and spatially dependent components (e.g., $T = \hat{T}^A + \tilde{T}^A$) in the along-shelf advective term (Austin, 1999), and noting from continuity that if sea-level changes are small ($\frac{\partial\eta}{\partial t} \sim 0$), then

$$\int\int\frac{\partial(v)}{\partial y}dA = \hat{u}H|_{x=-L}, \quad (2)$$

the heat budget equation (1) can be written as

$$\frac{\partial}{\partial t}\int\int\hat{T}^A dA = \int_{-L}^{0}\frac{Q}{\rho C_P}dx + \int_{-H}^{0}\tilde{u}\tilde{T}dz|_{x=-L} + \hat{u}H|_{x=-L}(\hat{T}-\hat{T}^A) - \frac{\partial\hat{T}^A}{\partial y}\int\int vdA - \int\int\frac{\partial(v\tilde{T}^A)}{\partial y}dA. \quad (3)$$

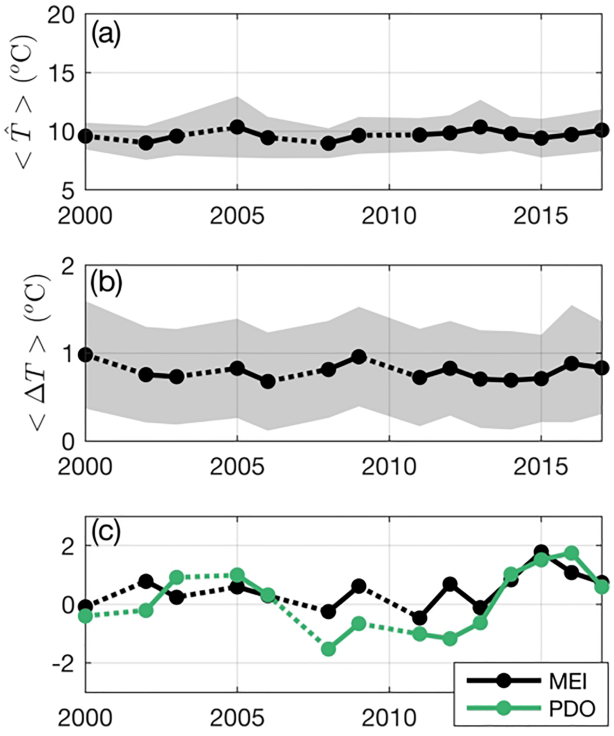

Figure 4. (a) Summer depth-averaged temperature at SH15, (b) surface-to-bottom thermal stratification, and (c) regional climate indices of the PDO and ENSO. Gray shading indicates the standard deviation of daily values each summer. Dashed lines span years without data.

The first term on the left hand side represents the temporal change in the heat content of the cross section. The first term on the right hand side is the heat flux through the surface, while the second term is the on/offshore flux of heat due to the depth-dependent flow (upwelling/downwelling). The third term represents the on/offshore eddy heat fluxes into the section, while the fourth term is the along-shelf heat flux associated with the section average along-shelf temperature gradient. Finally, the fifth term is the along-shelf heat flux due to spatially correlated variations in v and T. To express the results in terms of the effective temperature change over the inner shelf, equation (3) is integrated over time and divided by the inner-shelf area.

This study focuses on a potential balance between the first, second, and third terms in equation (3), which represent an along-shelf uniform, two-dimensional heat budget:

$$\frac{\partial}{\partial t}\int\int \hat{T}^A dA = \int_{-L}^{0} \frac{Q}{\rho C_P} dx + \int_{-H}^{0} \tilde{u}\tilde{T} dz|_{x=-L} - \epsilon, \tag{4}$$

where ϵ is the residual of the three-term balance. Previous assessments of the midshelf summer heat budget along the upwelling-favorable U.S. West Coast have found that across-shelf advection generally dominates along-shelf advection (Dever & Lentz, 1994; Rudnick & Davis, 1988). Thus, it is hypothesized here that a two-dimensional budget will capture the dominant controls on the inner-shelf temperature off Oregon. Furthermore, along-shelf gradients of temperature and along-shelf velocity, v, in the region of SH15 cannot be resolved from the available data. Temperature measurements at other PISCO sites, which were used to estimate an along-shelf heat flux, were only available in select years. The two-dimensional balance reduces all heat flux contributions from eddies or along-shelf gradients into the residual term. Methods for estimating each of the three terms explicitly calculated in this two-dimensional heat budget are described in the following sections.

2.5.1. Calculating the Inner-Shelf Temperature Change

Without temperature measurements further inshore of SH15, the temperature over the cross section was assumed to be constant with depth in the calculation of $\hat{T}^A$. As an approximation of the error associated with this assumption, we compare $\hat{T}^A$ to $\hat{T}$, which would be equivalent to $\hat{T}^A$ if the temperature was instead assumed to be constant along σ levels and if the depth was assumed to decrease linearly from H at $x = -L$ to 0 at the coast. The resulting summer mean temperature change is on average 17% (or 8×10^{-4} ° C day^{-1}) lower when the temperature is assumed to be constant with depth rather than along σ levels.

For this analysis, the across-shelf profile of the inner-shelf bathymetry was assumed to be linear (e.g., following the dashed line in Figure 1b). The impact of considering the full bathymetry on temperature variations (the first term in equations (3) and (4)) at this location is small. The approximation of a linear bathymetry results, on average, in an increase of less than 13% of the inner-shelf area estimated from a bathymetric profile. Regardless, the relationship between the surface and advective heat fluxes would not change, as the results reported here were divided by the estimate of the inner-shelf area, to place them in terms of the effective change in temperature over the inner shelf.

2.5.2. Across-Shelf Heat Flux Estimate

The depth-dependent across-shelf heat flux (the third term in equations (3) and (4)) was calculated at SH15 using profiles of $\tilde{T}$ and $\tilde{u}$ on the σ-coordinate grid (e.g., Figures 3c and 3d). The time series of $\tilde{u}$ used the linear surface extrapolation method above the depth where ADCP data are available, but a comparison to the well-mixed surface extrapolation is also discussed below.

2.5.3. Surface Heat Flux Estimate

Surface heat flux is both a critical component of the heat budget and requires observations not typically collected during monitoring efforts such as the PISCO program. Additionally, small uncertainties in this term can lead to large imbalances in the budget at seasonal timescales (Lentz, 2009). As there were no local measurements of surface heat flux over the record period, fields from the nearest ERA5 grid location were

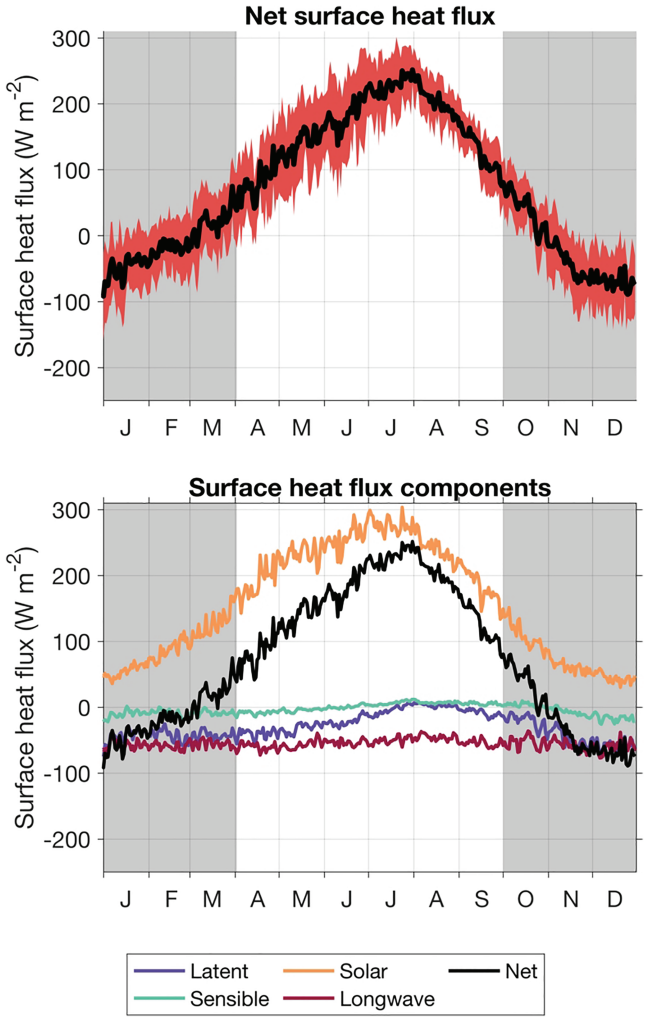

Figure 5. (a) The interannual mean of the daily net surface heat flux from the closest ERA5 location, with the standard deviation over the 16 study years shaded in red. (b) A climatology of the daily surface heat flux components and the net surface heat flux. Gray shading indicates times without summer observations.

used to estimate the net surface flux at SH15. Calculation of the net surface heat flux was approximated by assuming that the surface heat flux was uniform in the across-shelf distance from $x = -L$ to $x = 0$. However, an across-shelf gradient in SST could lead to an across-shelf gradient in the net surface heat flux. Although this could alter the results of the heat budget, it was possible to quantify the across-shelf surface heat flux variability with the data available.

2.5.4. Along-Shelf Heat Flux Estimate

For years when data were available, the along-shelf heat flux (term 5 in equation (3)) was estimated in order to determine whether an along-shelf gradient may balance the residual from the two-dimensional heat budget. A new residual,

$$\epsilon' = \epsilon - \frac{\partial \hat{T}^A}{\partial y} \int\int v dA, \tag{5}$$

was compared to the residual of the two-dimensional heat budget (equation (4)). The depth-averaged along-shelf velocity, $\hat{v}$, at SH15 was assumed to be representative of the along-shelf currents over the entire inner-shelf cross section. Similarly, depth-averaged temperatures were estimated by the mean of the four temperature measurements throughout the water column, and the depth average at the offshore boundary was assumed to be representative of the area-averaged inner-shelf temperature at each time. There are multiple stations in the PISCO array from which an along-shelf temperature gradient could be measured (Figure 1). It is not obvious a priori what length scale should be the most dynamically relevant, so results using along-shelf temperature differences between SH15 and SHN (a north-south separation of 1 km), SH15 and YB (a north-south separation of 8 km), and between SH15 and SR (a north-south separation of 28 km) were compared here. An estimate of the predicted temperature gradient, ΔT_{pred}, required to close the budget (such that $\epsilon' = 0$) at each of these length scales was also calculated. From equation (5),

$$\frac{\epsilon}{\int\int v dA}\Delta y \sim \frac{\epsilon}{\hat{v} < A >}\Delta y = \Delta T_{pred}. \tag{6}$$

3. Results

3.1. Terms in the Heat Budget

3.1.1. Summer Temperature Changes

The net summer trend of the depth-averaged temperatures ($\hat{T}$) measured at SH15 was not significantly different from zero (i.e., estimated from the daily means over the record for each year examined, Figure 2). While intermittent periods of warming or cooling at time scales from days to weeks existed in all years, the standard deviation from the summer mean was less than 2.5°C each year (Figure 4a). Interannual variability in inner-shelf temperature was also small (Figures 2 and 4a). The summer mean temperature ($< \hat{T} >$) was between 8.9 and 10.6°C, with a range of 1.7°C over the 14 years examined. The standard deviation in the summer mean temperature from year-to-year was 0.5 ° C, which was less than the standard deviation of the mean daily values for each year (1.6°C, on average). Why the interannual variance in mean inner-shelf temperatures was smaller than the intraseasonal variance is not obvious. The heat budget examined in the following sections has the potential to help understand why the summer temperature was so consistent from year-to-year.

3.1.2. Summer Surface Heat Flux

The net surface heat flux from the closest ERA5 grid location (Figure 1) had a strong seasonal cycle, in which the surface heat flux warmed the coastal ocean in the summer months (i.e., April–September) and cooled it in winter (Figure 5a). Note that the diurnal cycle is not represented in Figure 5, which shows the annual cycle of daily-averaged surface heat flux. Solar radiative heating dominates both the mean and the variance

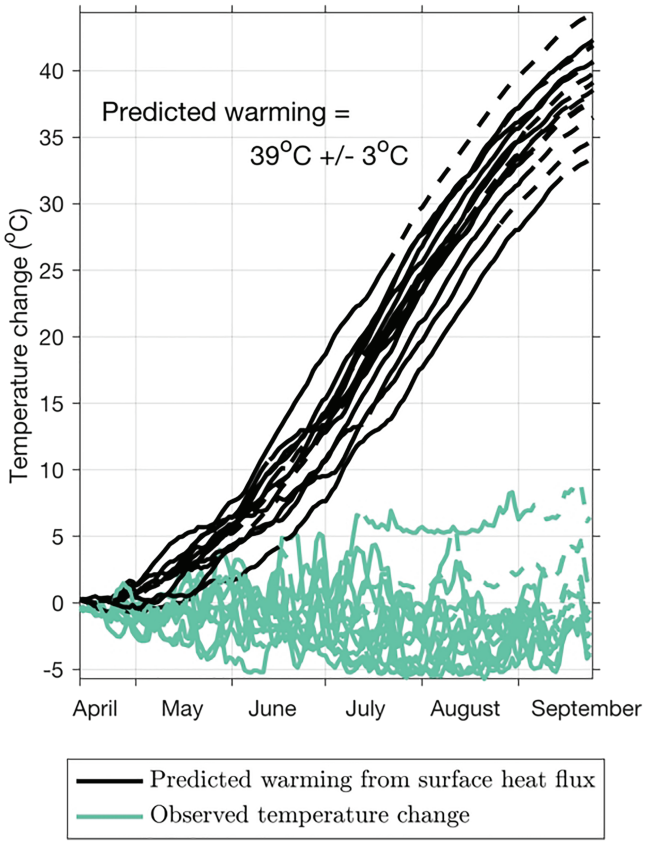

Figure 6. Net predicted summer warming from surface heat flux over the inner shelf from 13 April to 24 September (black). The net temperature change, from daily-averaged values, is also shown for comparison (green). Times where no SH15 data are available are replaced in the cumulative sum with the mean daily value across all record years, represented by dashed lines.

in the net surface heat flux (Figure 5b). Throughout most of the year, latent, sensible, and net longwave radiative heat fluxes act to cool the water column.

The estimated cumulative surface heat flux over the summer, using the ERA5 products along with the observed SST at SH15, was large, with a summer mean value across all years of $3.4 \times 10^4 \pm 4.9 \times 10^3$ W m^{-2}. In order to compare the influence of this heat flux on the water column onshore of SH15, we also estimate the equivalent temperature change associated with this heat flux by the cumulative time integral of $< A >^{-1} \int_{-L}^{0} Q(\rho C_P)^{-1} dx$. The predicted temperature change due to the cumulative surface heat flux over the summer was equivalent to an increase in the inner-shelf temperature of 39 ± 3 ° C (black lines, Figure 6). Note that this is not the temperature change that would be predicted (because an observed warming of the water column would change the air-sea temperature difference and alter the heat exchange) but is a demonstration of the amount of heat flux at the surface represented by an equivalent temperature change averaged over the water column. The interannual variability in the cumulative surface heat flux was small during the observational period. The standard deviation in the predicted summer warming at SH15 due to surface heat flux (3 ° C) was less than 8% of the interannual mean (39 ° C, e.g., Figure 6) but large compared to the observed temperature changes. In contrast to this predicted warming, over the same period the depth-averaged water temperature, $\hat{T}$, fluctuated by less than ∼5 ° C with a net summer change of −1.2 ± 2.9 ° C (Figures 6 and 2). Thus, it is clear that a one-dimensional heat budget without cooling from one of the advective terms in equation (3) does not close.

3.1.3. Summer Across-Shelf Heat Flux

The across-shelf heat flux at SH15 depends on correlations between depth-varying temperature and velocity, $\tilde{T}$ and $\tilde{u}$, respectively. The summer mean profile of depth-varying temperature ($< \tilde{T} >$) was stably stratified throughout the water column (Figure 3a). The summer mean profile of depth-varying across-shelf velocity ($< \tilde{u} >$) had an offshore current near the surface, an onshore flow at middle depth, and a weak offshore flow near the bottom (Figures 3b and 3d), suggesting a three-layer vertical profile. This complex summer mean structure was consistently observed in all years but was in contrast to the vertical structure of the dominant EOF mode of seasonal $< \tilde{u} >$ variability. The mode-one EOF profile, which captured most (74–82%) of the variance each year, had a two-layer structure more typical of upwelling dynamics, with offshore flow at the surface and onshore flow at depth. Further investigation of the dynamics and time dependence that lead to this summer mean structure are beyond the scope of this study. The primary mode of variability is mentioned here in order to emphasize that, despite the complex vertical structure of $< \tilde{u} >$ (Figures 3b and 3d), the dynamics at this site are consistent with patterns of wind-driven coastal upwelling.

The summer mean profile of the depth-varying across-shelf heat exchange, $< \tilde{u}\tilde{T} >$, revealed offshore advection of heat at the surface each summer (Figure 3e). This summer mean profile of the across-shelf heat flux was quantitatively similar to the product of the summer mean profiles $< \tilde{u} >$ and $< \tilde{T} >$ each year (Figures 3e and 3f), indicating that temporal variations in the temperature and across-shelf velocity are uncorrelated throughout each summer. Both profiles exhibit offshore heat flux near the surface, where the temperature anomaly was warm and the across-shelf currents were directed offshore. At middle depth, temperature anomalies, $< \tilde{T} >$, were close to zero (Figure 3a), and as a result, relatively little heat was exchanged in the across-shelf direction by the predominantly onshore flow (Figure 3b). Near the bottom, across-shelf velocities were small (Figure 3b), which contributed to relatively little heat being exchanged near the seafloor, despite the temperature anomaly. The vertical structure of the summer mean, depth-varying across-shelf heat flux (Figure 3e) diverges from a prototypical upwelling-driven heat flux, which would have an offshore flux of relatively warm water near the surface and an onshore flux of relatively cool water near the bottom.

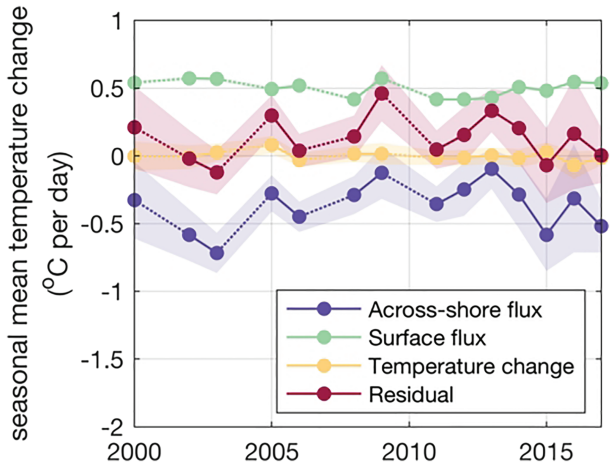

Figure 7. The summer mean of each term in a two-dimensional heat budget for the summer upwelling season, as well as the residual, for each year. Shading represents the standard mean error of the daily data. Dashed lines span years without data.

3.2. Summer Mean and Interannual Variability of the Heat Budget

The summer mean of the rate of temperature change (term 1), the surface heat flux (term 2), and the across-shelf heat flux (term 3) were calculated following equation (4) (Figure 7). Summer means were computed from daily-averaged values for all years except 2001 and 2010, where no data were available and years 2004 and 2007 with short record lengths. For each year, the residual of these three terms was assumed to represent the contributions of the remaining terms in equation (3). No significant mean summer temperature change is found for any year (Figure 7 and Table 1). In all years, the summer mean temperature change (5.1×10^{-5} ° C day^{-1}) was 3 orders of magnitude smaller than the contribution to the temperature change from the summer mean surface heat flux (0.5 ° C day^{-1}). The summer mean across-shelf heat flux contribution (−0.37 ° C day^{-1}) was similar in magnitude as surface heating in most years and appeared to buffer the inner shelf from warming due to the incoming surface heat flux each summer.

While across-shelf heat flux was a leading term in the summer heat budget along the Oregon coast, it also had the greatest interannual variability of all estimated terms (Figure 7 and Table 1). The summer mean contribution to cooling the inner shelf from the across-shelf heat flux varied between 0.1 and 0.72°C day^{-1}, with a standard deviation around 50% of the mean. The range of the across-shelf heat flux contribution was large, 0.62°C day^{-1}, compared to the range of the surface heat flux contribution and observed temperature change, both 0.15°C day^{-1}. Thus, the interannual variability in the residual term was predominately due to the interannual variability in the across-shelf heat flux.

Despite the large interannual variability in the across-shelf heat flux, the two-dimensional heat budget closed to within the standard error of the estimates in 11 out of 14 years (Figure 7). The residual was only significantly different from zero in 2005, 2009, and 2013. Over the 11 years that the heat budget closed, the residual was less than 20% of the leading terms. However, in 11 out of 14 years the interannul balance indicates that there is more surface heating than observed cooling due to the across-shelf heat flux. Even in those years when the two-dimensional heat budget did not balance, the temperature change was still zero. This suggests that, while the heat budget was predominantly two-dimensional in all years, an additional term such as the along-shelf heat flux would be required to close the budget, that the uncertainty in the across-shore heat flux is not fully represented by the mean standard error, or that there is a possible observational bias.

3.3. Departures From a Two-Dimensional Heat Budget

3.3.1. Uncertainty in the Across-Shelf Heat Flux

The largest source of uncertainty in the across-shelf heat flux (term 3 from equations (3) and (4)) was likely the lack of near-surface and near-bottom velocity measurements at SH15. At the surface, a linear extrapolation of the velocity using the slope of the top two values was used to estimate the summer heat budget (Figure 7, e.g.). As an estimate of the range of uncertainty associated with this approximation, the across-shelf heat flux was also calculated assuming a well-mixed approximation at the surface (see section 2.2.3). This resulted in a decrease in the summer mean across-shelf advective cooling of 0.19 ± 0.06 ° C day^{-1}

Table 1
Interannual Mean Temperature Change, Standard Deviation, and Range for Each Term in the Two-Dimensional Heat Budget, Reported in ° C day^{-1}

	Mean	*SD*	Min	Max
Temperature change	5.1×10^{-5}	0.03	−0.07	0.08
Surface flux	0.5	0.06	0.42	0.57
Across-shelf flux	−0.37	0.18	−0.72	−0.1
Residual	0.13	0.17	−0.17	0.43

Note. Statistics are calculated from summer means over 14 years.

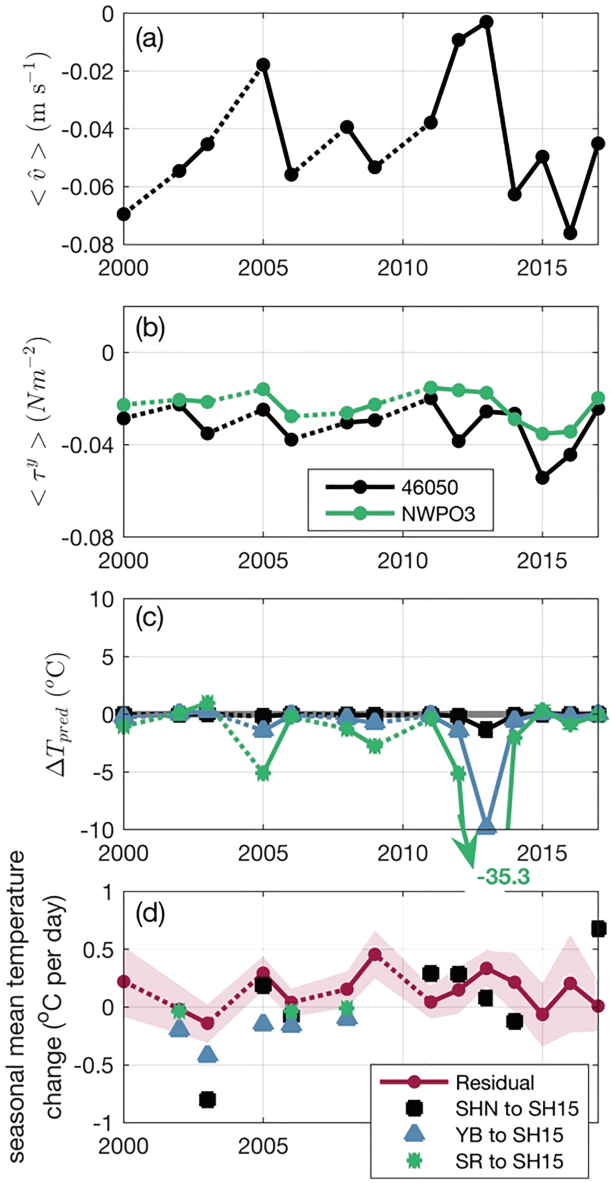

Figure 8. Summer mean, depth-averaged (a) along-shelf velocity at SH15, (b) along-shelf wind stress from NDBC buoy 46040, and (c) temperature difference between SH15 and three other PISCO stations at varying distances along the shelf. The gray shaded region indicates the accuracy range of the temperature sensors. (d) The residual from the two-dimensional heat budget (i.e., Figure 7) along with an estimate of the along-shelf heat flux using observed temperature gradients at three along-shelf length scales. Dashed lines span years without data.

over the 14 years, but the year-to-year variations were essentially unchanged. This decrease in the advective flux increased the magnitude of the residual in most years and resulted in 3 years where the across-shelf heat flux contributed to warming of the inner shelf. Given that warming of the inner shelf by an upwelling circulation is an unlikely result in a stably stratified upwelling-dominated system, we conclude that the linear extrapolation of surface velocities was likely a better approximation of the currents at the near-surface depths where measurements were not available.

3.3.2. Along-Shelf Heat Flux

This study focused on a two-dimensional heat budget, in which the along-shelf and eddy advection of heat were assumed small. While it was not possible to estimate the role of eddy advection within the data set to test this assumption, the temperature observations made at the other PISCO sites (Figure 1) provided an estimate of the along-shelf advective heat flux, which might account for the residual in the two-dimensional heat budget. In general, both the summer mean surface wind stress and the summer mean depth-averaged

along-shelf velocities were southward (Figures 8a and 8b). If the along-shelf heat flux was the remaining cooling process closing the heat budget, this would require a summer mean along-shelf temperature gradient with warmer waters to the south and cooler waters to the north. Assuming that the along-shelf inner shelf temperature gradient was uncorrelated with the along-shelf currents, the magnitude of the summer mean along-shelf temperature gradient required to close the heat budget was approximated following equation (6). The along-shelf temperature difference, ΔT_{pred}, increased with an increase in the along-shelf length scale, Δy (e.g., Figure 8c). Median values of ΔT_{pred} from stations SHN (1 km north of SH15), YB (8 km north), and SR (28 km north) to SH15 were −0.02, −0.17, and −0.62°C, respectively, with negative values indicating cooler temperatures to the north. The more localized predicted summer mean temperature differences were within the instrument error and cannot be resolved from the observations.

An estimate of the along-shelf heat flux was calculated for years with overlapping depth-averaged temperatures observations at each station pair for at least 50% of the summer (Figure 8d). Using the observed temperature gradient between stations SHN and SH15 resulted in a highly variable estimate with fluctuations on the same order of magnitude as the surface and across-shelf heat fluxes themselves. This was likely a function of the accuracy of the temperature sensors themselves. The along-shelf heat flux estimated from the temperature gradient between stations YB and SH15 contributed to cooling the water column and slightly increased the magnitude of the residual. Although the summer mean temperature differences between stations SR and SH15 were large enough to be well resolved most years of this study, the heat flux contribution calculated at this 28-km along-shelf length scale was negligible. Thus, a large-scale (order 28 km or greater) summer mean temperature gradient does not significantly impact the heat budget at SH15. However, along-shelf temperature gradients at length scales of $\mathcal{O}$(10 km) or less may be important to the heat budget during some years.

4. Discussion

These results confirm that, at minimum, a two-dimensional heat budget was required to close the seasonally averaged heat balance of the Oregon inner shelf (e.g., Figure 6). During the summer upwelling season examined, heating from the surface was predominantly balanced by cooling from the across-shelf advective flux. However, the balance did not close in all years examined, suggesting that either additional terms were required to fully close the heat balance or the uncertainty of the across-shelf advective term was both large and variable on interannual timescales. Additionally, it is not clear what dynamically drives the across-shelf advective term to buffer the surface heat flux as it does. The uncertainty in the across-shelf flux term, its drivers, and potential explanations for its interannual variability are discussed below in more detail.

The envelope of uncertainty in the across-shelf advective term was often large relative to the size of the term itself and was the main source of variance to the interannual heat balance (Figure 7). This variance could potentially result from variability in the observational period each summer. Here summer mean values were reported as the average over the observational period in each summer. However, there was substantial variability in the record length from year-to-year (e.g., Figure 1). For example, in 2000 and 2016 there were no available data until July. While these differences in observational period could lead to a sampling bias, we suggest that it is either small, as neither of the two years highlighted above, 2000 or 2016, stands out as anomalous within this analysis, or should be random within the interannual means and therefore be represented in the two-dimensional residual (Figure 7). Second, most of the across-shelf heat flux at SH15 occurred near the surface of the water column (e.g., Figure 3e). Therefore, the across-shelf heat flux was sensitive to the velocity extrapolation over the first 2–3 m of water depth (e.g., Figure 3). This uncertainty was minimized as much as possible by both requiring that the temperature is resolved over the full water column and using the linear velocity extrapolation to the surface. Previous works (Kirincich et al., 2005) using the PISCO data set have shown that across-shelf surface layer transports estimated using linear extrapolation to the surface had the highest correlations to the theoretical wind-driven across-shelf transport. This represents a reasonable metric for the Oregon shelf, with its predominantly wind-driven circulation.

It is not clear from this analysis what, dynamically, drives the summer mean across-shelf heat flux to balance the surface heat flux in most years. Even in the years where this two-dimensional heat budget did not close, it was curious that the summer mean depth-averaged temperatures were consistent from year-to-year, indicating that the net advective heat fluxes balanced the surface heat flux. Perhaps there is a feedback mechanism, such as proposed in the conceptual model by Fewings and Lentz (2011), whereby the across-shelf

heat flux decreases the temperature stratification resulting in a decrease in the heat flux over time even if the strength of the circulation is unchanged. There may also be a small-scale relationship between the air-sea temperature difference and humidity or cloud formation which may lead to a local reduction in the surface heat flux that might not be represented in the ERA5 gridded output. The intraseasonal variations of the two-dimensional balance are the subject of ongoing work using the PISCO data set. Furthermore, the barotropic across-shelf heat flux (term 4 in equation (3)) due to eddies or rip currents could contribute to the heat budget variability at this site although these advective fluxes cannot be constrained by the observations herein.

Additionally, seasonally averaged fields that might be related to the heat flux over the inner shelf were examined to aid interpretation of the interannual variability in the summer heat budget (Figure 7). Previous works in the region (Kirincich et al., 2005) have shown that across-shelf exchange is strongly correlated with along-shelf wind stress as well as with stratification during the summer upwelling season on the timescales of wind events. However, there was no significant correlation between the across-shelf heat flux and the along-shelf wind stress at the nearest offshore and nearshore buoy locations nor the top-to-bottom temperature difference at SH15 (Figures 8b and 4b) on seasonal timescales. While it is likely that intraseasonal variations in the along-shelf wind stress and temperature stratification are related to the across-shelf heat flux on the timescales of wind events (Allen et al., 1995; Austin & Lentz, 2002), this was not evident in the summer mean.

Finally, the interannual variability of the two-dimensional budget residual might be the result of larger-scale regional climate variability. While the PISCO mooring record was too short to quantitatively examine climate-scale trends, the summer mean of the PDO (http://research.jisao.washington.edu/pdo/PDO.latest) and of the ENSO Multivariate Index (MEI; https://www.esrl.noaa.gov/psd/enso/mei/) were examined for their potential consistency with the interannual heat budget record (Figure 4c). Over the 16-year period both indices were weakly correlated with the along-shelf wind stress (not shown here) but had variability that did not correspond with changes in the two-dimensional residual. For example, the positive anomaly in both the PDO and ENSO that occurred from 2014 to 2016 (Figure 4c) did not correspond with anomalous results in the heat budget (Figure 7). This result has implications in predicting the net impact of different climate change scenarios on coastal ocean temperature trends and variability, which is an important parameter for understanding and predicting the biological and ecological response over the inner shelf coastal region.

5. Conclusions

Examining a long-term record of inner shelf summer observations, the depth-averaged temperature in 15 m of water along the Oregon shelf was relatively constant from April to September, with a standard deviation of less than 2.5°C each year, despite strong surface heating. Summer mean temperatures were also consistent year-to-year, with a standard deviation of 0.5°C. In 11 out of 14 years, the across-shelf advective cooling was sufficient to buffer the inner shelf from the surface warming, and the two-dimensional heat budget closed within the mean standard error. However, the cooling contribution from the across-shore heat flux had an interannual range that was large (0.62°C day^{-1}) compared to the range in the warming contribution of the surface heat flux and the range of the observed temperature change (both 0.15°C day^{-1}). While the balance between surface warming and across-shore cooling can be sufficient to maintain the inner-shelf temperatures in many of the years examined, either along-shelf or eddy advection must also be present in a number of years to maintain the temperatures observed. In these years, the mean summer heat budget was three-dimensional. Further investigation is needed in order to understand the intraseasonal dynamics that lead to this year-to-year variability.

Appendix A: Surface Heat Flux Products

Measuring and calculating the terms that contribute to the net surface heat flux is a challenge in coastal oceanography. Measurements of radiation heat fluxes and air humidity are difficult to make and have sparse coverage globally (Yu, 2019), although spatial variability in surface heat flux can have a significant impact on temperature gradients (Tozuka et al., 2018). Measurements of radiation heat fluxes and air humidity were not collected as part of the PISCO program, and there were no local sources of these data that spanned the PISCO collection period. Therefore, this analysis relied on reanalysis products to estimate the surface heat

Table A1
An Overview of the Spatial and Temporal Resolution of Surface Heat Flux Reanalysis Sources Near Site SH15

Source	Grid center	Grid size	Time range	a	b	R^2
NCEP	−125.63°, 44.76°	2°	1948–nrt	0.75 ± 0.02	3.12 ± 0.29	0.61
OAFlux	−124.5°, 44.5°	1°	1985–2009	0.88 ± 0.02	1.52 ± 0.19	0.82
ERA_a	−124.5°, 44.75°	0.25°	1979–nrt	0.92 ± 0.01	1.3 ± 0.12	0.85
ERA_b	−124.25°, 44.25°	0.25°	1979–nrt	0.46 ± 0.02	6.99 ± 0.26	0.6[a]

Note. The parameters a, b, and the coefficient of determination, R^2, are results of a linear regression comparison of the reanalysis SST to the measured SST from NDBC buoy 46050.
[a]Comparison is between ERA_b reanalysis SST and measured SST from SH15.

flux component in the heat budget. A comparison of some of the available products is included here as a justification of the choice to use the ERA5 product and as a discussion of the uncertainty associated with this choice.

Three global surface heat flux reanalysis products were compared: the NOAA National Center for Environmental Prediction (NCEP)/NCAR Reanalysis 1 (Kalnay et al., 1996), the Woods Hole Oceanographic Institution Objectively Analyzed air-sea Fluxes (OAFlux; http://oaflux.whoi.edu), and the ECMWF ERA5 data set (Forecasts, 2019). The NCEP reanalysis data were available daily or four times daily on a 192 × 94 global grid from 1948 to near real time (nrt; Table A1). The nearest oceanic grid point to SH15 was far offshore in over 2,800 m of water depth (Figure A1). OAFlux had a finer (1°) resolution, with a grid center nearer to SH15 on the 100-m isobath and provided surface heat flux estimates daily from 1985 to 2009 (Table A1).

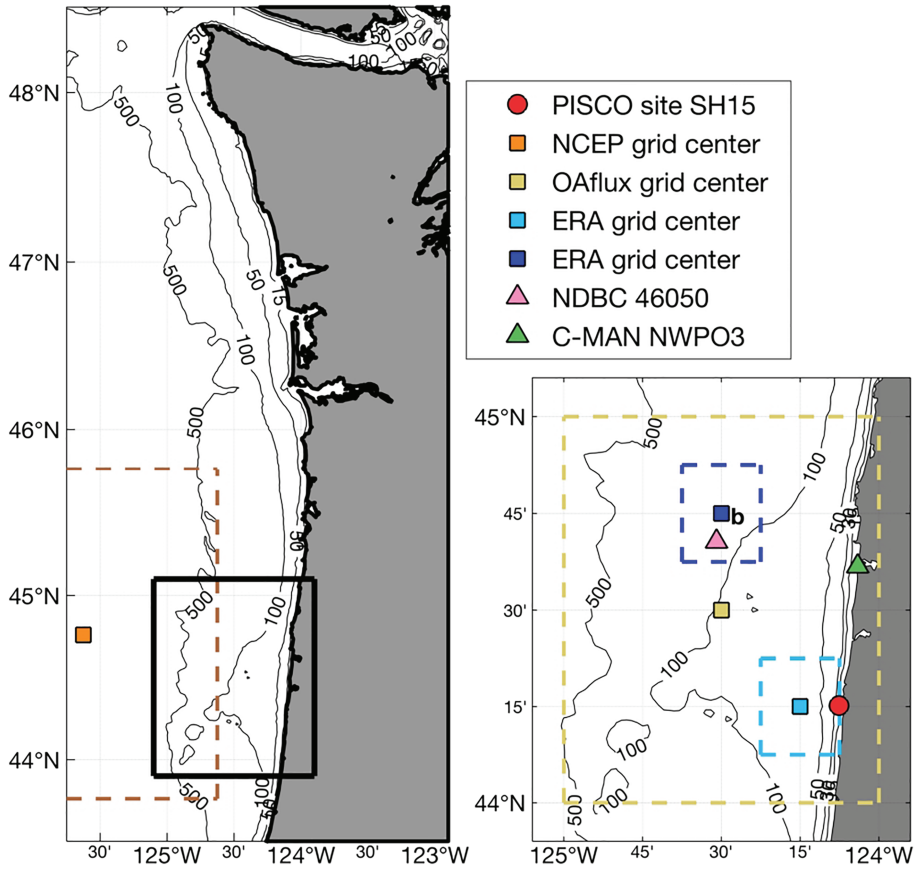

Figure A1. The location and resolutions of the nearest grid points from each reanalysis product, relative to NDBC buoy 46050, CMAN station NWPO3, and SH15.

Table A2
The Time-Integrated Surface Heat Flux From April to September from Different Surface Heat Flux Sources

Source	Mean	*SD*
NCEP	37.27	2.01
OAFlux	36.18	2.02
ERA_a	34.03	2.66
ERA_b	40.43	2.58

Note. Units are °C day^{-1}, following equation (A1). Statistics are computed from seasonal mean values from 1999 to 2008.

The recently released ERA5 product had the finest spatial and temporal resolution with surface heat flux reported hourly from 1979 to nrt on a 0.25° global grid.

The cumulative time integral of the surface heat flux was compared between each of these sources over 10 years (Table A2). The surface heat flux was presented in terms of the predicted temperature change of the water column onshore of SH15, in ° C day^{-1}, by

$$Q' = \frac{Q}{\rho_o C_P H_{7.5}}, \tag{A1}$$

where $H_{7.5} \equiv 7.5$ m is an estimate of the mean depth inshore of SH15. The period from 1999 to 2008 was chosen to coincide with available measurements at SH15 as well as the extent of OAFlux availability. ERA_a, which is located closest to NDBC buoy 46050 (Figure A1), and ERA_b, located nearest SH15, are both shown to demonstrate the spatial variability in surface heat flux at the subdegree scale. The mean and standard deviation of the summer mean surface heat flux contribution to the temperature change across the 10 years were 37.27 ± 2.01, 36.18 ± 2.02, 34.03 ± 2.66, and 40.43 ± 2.58°C day^{-1} for NCEP, OAFlux, ERA_a, and ERA_b, respectively. The interannual variability was the greatest for the two ERA locations. This could be related to the smaller grid size, which may reduce the amount of spatial filtering of the data sources. The cumulative predicted change in temperature from OAFlux fell between the two ERA predictions, which were both contained within the spatial range of the same OAFlux grid cell.

Due to the sparseness of observational data in this region, the accuracy of each of these products could not be assessed directly. As a proxy, a comparison of the SST from each of these reanalysis products to the SST measured at the nearby NDBC buoy 46050 was used to assess how well the surface temperature changes were represented by each reanalysis. NDBC buoy 46050 is located in greater than 100 m of water, at roughly the same longitude as ERA_a and the nearest OAFlux grid center to SH15. A linear regression fit between each product and measured SST was applied, following $SST_r = aSST_o + b$ (Table A1). Subscripts r and o refer to reanalysis values and observations from NDBC buoy 46050, respectively. A comparison of the reported SST from ERA_b to the top temperature at SH15 is also included. In addition, a time series of SST is shown from 2003 to visually compare results between these sources (Figure A2).

The reanalysis SST was highly correlated with surface observations ($R^2 \geq 0.6$). The regression intercept, b, was greater than 0, indicating that the observations were cooler, on average, than the reanalysis data

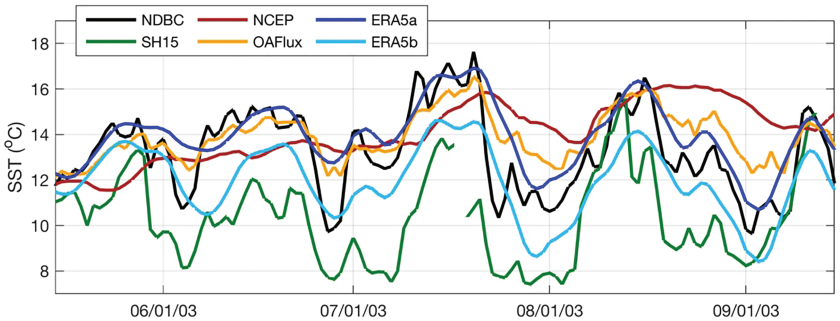

Figure A2. A time series of SST from each reanalysis product is compared to SST observed from NDBC buoy 46050 and SH15 over the summer season in 2003 (selected for the temporal coverage of SH15 observations).

(Table A1). The regression slope, a, was less than 1, indicating a greater temperature range in the observations as well. Further onshore, the SST was cooler, and the temperature range was greater (Figure A2). The comparison between SST from ERA5$_a$ and from NDBC buoy 46050 was most similar, with the highest R^2 coefficient of determination as either of the other two reanalysis products. Although statistically the linear fit between SST from ERA5$_b$ and at SH15 was less robust than the offshore sites, the comparison between ERA5$_a$ and NDBC buoy 46050 provides confidence that this was the best estimate available of local surface heat flux in the vicinity of SH15. Based on this analysis, the ERA5 product was chosen for the surface heat flux calculation. In order to further account for the impact that the observed across-shelf gradient in SST had on the outgoing longwave, latent, and sensible heat flux components, each of these terms was recalculated from fields from the ERA5 reanalysis following the COARE algorithm (Fairall et al., 2003), replacing the ERA5 SST with the SST from PISCO measurements.

Acknowledgments
The authors would like to acknowledge the David and Lucile Packard Foundation and The Gordon and Betty Moore Foundation for their support of the Partnership for Interdisciplinary Studies of Coastal Oceans (PISCO) mooring program. This paper is PISCO contribution 504. The contributions of A. Kirincich and S. Lentz were supported by National Science Foundation (NSF) Grant OCE-1558874). E. Lemagie was partially supported by NSF Grant OCE-1558874 as well as the Woods Hole Oceanographic Institution Postdoctoral Scholars program. Temperature and velocity data were collected and made available by PISCO (www.piscoweb.org). The NDBC and NWPO3 buoy data are freely available from NOAA (www.ndbc.noaa.gov). Surface heat flux reanalyses were download online: ERA5 was accessed through www.ecmwf.int/en/forecasts/datasets/reanalysis-datasets/era5, and NCEP and OAFlux data were downloaded from www.esrl.noaa.gov/psd/data/gridded/data.ncep.reanalysis.html and http://oaflux.whoi.edu/, respectively.

References

Allen, J. S., Newberger, P. A., & Federiuk, J. (1995). Upwelling circulation on the Oregon continental shelf. Part I: Response to idealized forcing. *Journal of Physical Oceanography*, *25*(8), 1843–1866. https://doi.org/10.1175/1520-0485(1995)025<1843:UCOTOC>2.0.CO;2

Austin, J. A. (1999). The role of the alongshore wind stress in the heat budget of the North Carolina inner shelf. *Journal of Geophysical Research*, *104*, 18,187–18,203. https://doi.org/10.1029/1998JC900122

Austin, J. A., & Lentz, S. J. (2002). The inner shelf response to wind-driven upwelling and downwelling. *Journal of Physical Oceanography*, *32*(7), 2171–2193. https://doi.org/10.1175/1520-0485(2002)032<2171:TISRTW>2.0.CO;2

Barth, J. A., Menge, B. A., Lubchenco, J., Chan, F., Bane, J. M., Kirincich, A. R., et al. (2007). Delayed upwelling alters nearshore coastal ocean ecosystems in the northern California current. *Proceedings of the National Academy of Sciences*, *104*(10), 3719–3724. https://doi.org/10.1073/pnas.0700462104

Bryden, H. L., Halpern, D., & Pillsbury, R. D. (1980). Importance of eddy heat flux in a heat budget for Oregon coastal waters, *85*, 6649–6653. https://doi.org/10.1029/JC085iC11p06649

Bylhouwer, B., Ianson, D., & Kohfeld, K. (2013). Changes in the onset and intensity of wind-driven upwelling and downwelling along the North American Pacific coast, *118*(5), 2565–2580. https://doi.org/10.1002/jgrc.20194

Cook, T., Folli, M., Klinck, J., Ford, S., & Miller, J. (1998). The relationship between increasing sea-surface temperature and the northward spread of Perkinsus marinus (Dermo) disease epizootics in oysters. *Estuarine, Coastal and Shelf Science*, *46*(4), 587–597. https://doi.org/10.1006/ecss.1997.0283

Dever, E. P., & Lentz, S. J. (1994). Heat and salt balances over the northern California shelf in winter and spring. *Journal of Geophysical Research*, *99*, 16,001–16,017. https://doi.org/10.1029/94JC01228

Di Lorenzo, E., & Mantua, N. (2016). Multi-year persistence of the 2014/15 North Pacific marine heatwave. *Nature Climate Change*, *6*(11), 1042–1047. https://doi.org/10.1038/nclimate3082

European Centre for Medium-Range Weather Forecasts (2019). ERA5 reanalysis (0.25 degree latitude-longitude grid). https://doi.org/10.5065/BH6N-5N20

Fairall, C. W., Bradley, E. F., Hare, J. E., Grachev, A. A., & Edson, J. B. (2003). Bulk parameterization of air-sea fluxes: Updates and verification for the COARE algorithm. *Journal of Climate*, *16*(4), 571–591. https://doi.org/10.1175/1520-0442(2003)016<0571:BPOASF>2.0.CO;2

Fewings, M. R., & Lentz, S. J. (2011). Summertime cooling of the shallow continental shelf. *Journal of Geophysical Research*, *116*, C07015. https://doi.org/10.1029/2010JC006744

Frischknecht, M., Münnich, M., & Gruber, N. (2015). Remote versus local influence of ENSO on the California current system. *Journal of Geophysical Research: Oceans*, *120*, 1353–1374. https://doi.org/10.1002/2014JC010531

Gentemann, C. L., Fewings, M. R., & GarcaReyes, M. (2016). Satellite sea surface temperatures along the West Coast of the United States during the 2014–2016 northeast Pacific marine heat wave. *Geophysical Research Letters*, *44*, 312–319. https://doi.org/10.1002/2016GL071039

Gill, A. E. (1982). *Atmosphere-ocean dynamics*. New York, NY: Academic Press.

Gordon, R. L. (1996). Acoustic Doppler current profiler: Principles of operation, a practical primer, second edition for broadband ADCPs.

Hickey, B., Geier, S., Kachel, N., Ramp, S., Kosro, P. M., & Connolly, T. (2016). Alongcoast structure and interannual variability of seasonal midshelf water properties and velocity in the northern California Current System. *Journal of Geophysical Research: Oceans*, *121*, 7408–7430. https://doi.org/10.1002/2015JC011424

Huyer, A. (1977). Seasonal-variation in temperature, salinity, and density over continental-shelf off Oregon. *Limnology and Oceanography*, *22*(3), 442–453. WOS:A1977DH78500007.

Huyer, A. (1983). Coastal upwelling in the California Current system. *Progress in Oceanography*, *12*(3), 259–284. https://doi.org/10.1016/0079-6611(83)90010-1

Huyer, A., Sobey, E., & Smith, R. (1979). Spring transition in currents over the Oregon continental-shelf. *Journal of Geophysical Research*, *84*, 6995–7011. https://doi.org/10.1029/JC084iC11p06995

Kalnay, E., Kanamitsu, M., Kistler, R., Collins, W., Deaven, D., Gandin, L., et al. (1996). The NCEP/NCAR 40-year reanalysis project. *Bulletin of the American Meteorological Society*, *77*(3), 437–472. https://doi.org/10.1175/1520-0477(1996)077<0437:TNYRP>2.0.CO;2

Keller, A. A., Oviatt, C. A., Walker, H. A., & Hawk, J. D. (1999). Predicted impacts of elevated temperature on the magnitude of the winter-spring phytoplankton bloom in temperate coastal waters: A mesocosm study. *Limnology and Oceanography,44*(2), 344–356. https://doi.org/10.4319/lo.1999.44.2.0344

Kirincich, A. R., Barth, J. A., Grantham, B. A., Menge, B. A., & Lubchenco, J. (2005). Wind-driven inner-shelf circulation off central Oregon during summer. *Journal of Geophysical Research*, *110*, C10S03. https://doi.org/10.1029/2004JC002611

Lentz, S. J. (1987). A heat budget for the northern California shelf during CODE 2. *Journal of Geopysical Research*, *92*, 14,491–14,509. https://doi.org/10.1029/JC092iC13p14491

Lentz, S. J. (1994). Current dynamics over the northern California inner shelf. *Journal of Physical Oceanography*, *24*(12), 2461–2478. https://doi.org/10.1175/1520-0485(1994)024<2461:CDOTNC>2.0.CO;2

Lentz, S. J. (2001). The influence of stratification on the wind-driven cross-shelf circulation over the North Carolina shelf. *Journal of Physical Oceanography*, *31*(9), 2749–2760. https://doi.org/10.1175/1520-0485(2001)031<2749:TIOSOT>2.0.CO;2

Lentz, S. J. (2009). The mean along-isobath heat and salt balances over the Middle Atlantic Bight continental shelf. *Journal of Physical Oceanography*, *40*(5), 934–948. https://doi.org/10.1175/2009JPO4214.1

Lentz, S. J., Beardsley, R. C., Irish, J. D., Manning, J., Smith, P. C., & Weller, R. A. (2003). Temperature and salt balances on Georges Bank February–August 1995. *Journal of Geophysical Research*, *108*(C11), 8006. https://doi.org/10.1029/2001JC001220

Lentz, S. J., Churchill, J. H., Marquette, C., & Smith, J. (2012). Evaluation and recommendations for improving the accuracy of an inexpensive water temperature logger. *Journal of Atmospheric and Oceanic Technology*, *30*(7), 1576–1582. https://doi.org/10.1175/JTECH-D-12-00204.1

Pierce, S. D., Barth, J. A., Thomas, R. E., & Fleischer, G. W. (2006). Anomalously warm July 2005 in the northern California Current: Historical context and the significance of cumulative wind stress. *Geophysical Research Letters*, *33*, L22S04. https://doi.org/10.1029/2006GL027149

Rudnick, D. L., & Davis, R. E. (1988). Mass and heat budgets on the northern California continental shelf. *Journal of Geophysical Research*, *93*, 14,013–14,024. https://doi.org/10.1029/JC093iC11p14013

Sanford, E. (1999). Regulation of keystone predation by small changes in ocean temperature. *Science*, *283*(5410), 2095–2097. https://doi.org/10.1126/science.283.5410.2095

Send, U. (1989). The origin of eddy heat fluxes in the northern California upwelling regime. *Journal of Geophysical Research*, *94*, 871–876. https://doi.org/10.1029/JC094iC01p00871

Smith, R. L., Huyer, A., & Fleischbein, J. (2001). The coastal ocean off Oregon from 1961 to 2000: Is there evidence of climate change or only of Los Niños? *Progress in Oceanography*, *49*(1), 63–93.

Somero, G. N. (2005). Linking biogeography to physiology: Evolutionary and acclimatory adjustments of thermal limits. *Front Zool*, *2*(1), 1.

Suanda, S. H., Barth, J. A., & Woodson, C. B. (2011). Diurnal heat balance for the northern Monterey Bay inner shelf. *Journal of Geophysical Research*, *116*, C09030. https://doi.org/10.1029/2010JC006894

Summerhayes, C. P., Emeis, K.-C., Angel, M. V., Smith, R. L., & Zeitzschel, B. (1995). *Upwelling in the ocean: Modern processes and ancient records*. New York, NY: Wiley.

Sydeman, W. J., Bradley, R. W., Warzybok, P., Abraham, C. L., Jahncke, J., Hyrenbach, K. D., et al. (2006). Planktivorous auklet Ptychoramphus aleuticus responses to ocean climate, 2005: Unusual atmospheric blocking? *Geophysical Research Letters*, *33*, L22S09. https://doi.org/10.1029/2006GL026736

Tozuka, T., Ohishi, S., & Cronin, M. F. (2018). A metric for surface heat flux effect on horizontal sea surface temperature gradients. *Climate Dynamics*, *51*(1), 547–561. https://doi.org/10.1007/s00382-017-3940-2

Yu, L. (2019). Global air-sea fluxes of heat, fresh water, and momentum: Energy budget closure and unanswered questions. *Annual Review of Marine Science*, *11*(1), 227–248. https://doi.org/10.1146/annurev-marine-010816-060704